DR. XUBO LIN (Orcid ID : 0000-0002-4417-3582)

Received Date : 27-Mar-2018

Revised Date : 01-Jun-2018

Accepted Date : 26-Jun-2018

Article type : Research Letter

Roles of PIP2 in the Membrane Binding of MIM I-BAR: Insights from Molecular Dynamics Simulations

Xubo Lin[1,2], Hongyin Wang[3,#], Zhichao Lou[2,4,#], Meng Cao[2,5,#], Zuoheng Zhang[2,5], Ning Gu[2,5,*]

1. Beijing Advanced Innovation Center for Biomedical Engineering, School of Biological Science and Medical Engineering, Beihang University, Beijing 100083, China.
2. State Key Laboratory of Bioelectronics, Jiangsu Key Laboratory for Biomaterials and Devices, School of Biological Sciences & Medical Engineering, Southeast University, Nanjing 210096, China.
3. Department of Integrative Biology and Pharmacology, McGovern Medical School, The University of Texas Health Science Center at Houston, Texas 77030, USA
4. College of Materials Science and Engineering, Nanjing Forestry University, Nanjing 210037, China.
5. Collaborative Innovation Center of Suzhou Nano-Science and Technology, Suzhou Key Laboratory of Biomaterials and Technologies, Suzhou 215123, China.

* Corresponding author. Phone/Fax: +86-025-83794960; E-mail: guning@seu.edu.cn

[#] These authors contribute equally. The authors declare no competing financial interest.

This article has been accepted for publication and undergone full peer review but has not been through the copyediting, typesetting, pagination and proofreading process, which may lead to differences between this version and the Version of Record. Please cite this article as doi: 10.1002/1873-3468.13186

TOC graphics

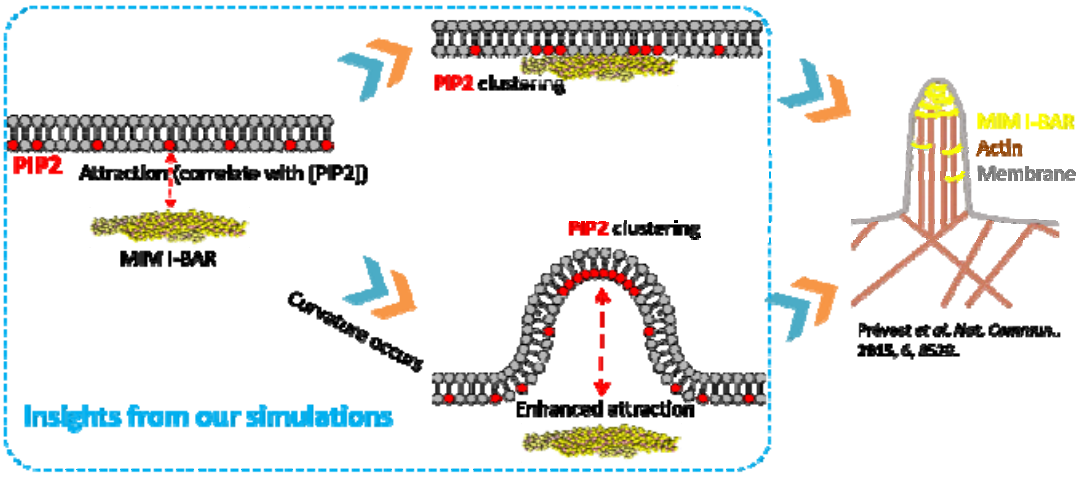

PIP2 is critical for MIM I-BAR-mediated membrane protrusion generation.

Significance Statement:

Homo sapiens MIM (missing-in-metastasis) I-BAR is supposed to be critical in sensing and generating membrane curvature, which determines the metastatic ability of cells. However, the detailed roles of phosphatidylinositol 4, 5-bisphosphate (PIP2) in this process is still far from clear. In this work, using multiple 10μs-scale coarse-grained molecular dynamics simulations, we reveal the following: **(1)** Compared to anionic POPS lipids, PIP2 plays predominant roles in the membrane binding of MIM I-BAR by contributing much higher local surface charge density, **(2)** MIM I-BAR has PIP2-binding sites on the surface (especially its ends), which explains the local PIP2 clustering around its membrane binding sites, **(3)** Membrane curvature may induce the re-distribution of lipids in the membrane and result in the local enrichment of PIP2 at membrane regions with negative curvature. Our findings may help elucidate how MIM I-BAR senses negatively curved membranes.

Abstract

In order to probe the roles of PIP2 in the interactions between MIM I-BAR and model membranes, we performed a series of 10μs-scale coarse-grained molecular dynamics simulations. Our results indicate that PIP2 plays predominant roles in the membrane binding of MIM I-BAR in a concentration-dependent manner and via electrostatic interactions. Besides, we find that the occurrence of the membrane curvature may induce the re-distribution of lipids in the membrane and result in the local enrichment of PIP2 at negatively curved membrane areas. Combining these roles of PIP2 in the membrane binding of MIM I-BAR helps explain how MIM I-BAR senses negative curvature and, thus, contributes to maintaining membrane protrusions.

1. Introduction

Membrane remodeling plays a key role in regulating various biological processes including membrane invaginations (e.g. endocytosis) and protrusions (e.g. filopodia). To fulfill the whole membrane remodeling process, many proteins such as cytoskeleton, actin, Bin-Amphiphysin-Rvs (BAR) proteins will be involved. It is reported that BAR proteins participate in sensing and generating the membrane curvature.[1-4] According to their preferences to membranes of different curvatures, BAR proteins are classified into three categories: N-BAR, F-BAR and I-BAR. N-BAR, which contains an N-terminal amphipathic helix, prefers membranes of high positive curvature[5]. F-BAR, the abbreviation of Fes/CIP4 homology BAR, has a wide preference to positively curved membranes[6]. I-BAR or inverse BAR is the only kind of BAR proteins that prefers the membrane of negative curvature[7]. However, compared to N-BAR and F-BAR[8-11], more efforts are still needed to study molecular-level interactions between I-BAR and lipid membranes.

Missing-in-metastasis suppressor 1 (MIM/MTSS1), which contains an I-BAR domain, plays an important role in regulating the cell metastatic ability.[12-14] It is widely reported in patients/animals that the MIM gene expression is negatively correlated to the metastasis ability of several cancer cells (e.g. bladder, breast and gastric cancer cells).[15-18] In order to understand the role of MIM I-BAR in membrane remodeling, Lee *et al*. resolved the crystal structure of MIM I-BAR and found that MIM I-BAR exist in the form of a dimer.[19] The dimer may be the functional form of MIM I-BAR proteins, since our previous studies also pointed out that inhibiting the dimerization of MIM I-BAR can significantly weaken MIM-mediated membrane protrusions.[20-22] Hence, in the current work, we only focus on the MIM I-BAR dimer. Besides, through systematic protein mutation experiments, Mattila *et al*. revealed the PIP2 (also known as $PI(4,5)P_2$, phosphatidylinositol 4, 5-bisphosphate)- and F-actin- binding sites of MIM I-BAR,[7] which is very important for understanding the role of MIM I-BAR in membrane remodeling. However, PIP2 is one kind of minor phospholipids (<5%) and its precursor (phosphatidylinositol, PtdIns) typically accounts for less than 15% of the total phospholipids located in intracellular membranes of eukaryotic cells.[23] Whether other major anionic lipids (e.g. phosphatidylserine, PS lipids) can have the similar role as PIP2 in the membrane binding process of MIM I-BAR is still unknown.

On the other hand, the mechanism how MIM I-BAR is selectively recruited onto the negatively curved membranes remains largely unexplored. As mentioned above, certain lipids play important roles in the membrane binding of MIM I-BAR. And lipids can differentially aggregated at membrane regions of different curvatures as indicated by large scale molecular dynamics (MD) simulations of complex membrane systems.[24] Hence, we hypothesize that membrane curvature induced re-distribution of these key lipids may provide an appropriate mechanism for MIM I-BAR's sensing membranes of the negative curvature. In order to test this hypothesis, we aim to quantify the exact preference of these lipids to different curvatures.

MD simulation provides a powerful tool to obtain molecular level interaction information, which is useful to elucidate the molecular mechanisms of many biological processes as an alternative tool to the experiments.[25-26] Hence, in this work, we perform a series of coarse-grained (CG) MD simulations to probe predominant roles of PIP2 in the membrane binding process of MIM I-BAR as well as the molecular mechanism of how MIM I-BAR senses membranes with negative curvature.

2. Methods

Molecular Dynamics Simulations. CG model, which maps several heavy atoms into one interaction site, allows MD simulations to study the biological processes with longer time and larger length scales. As one of the popular CG models for biological systems, Martini CG model has been widely used to study lipid membranes and proteins.[27-30] In this work, all simulations were performed with the Martini CG force field (version 2.1)[31] using GROMACS 5.0.4[32]. The initial membrane systems were built using the tool *insane* developed by Wassenaar *et al.*[33] The membrane systems with MIM I-BAR contain 3870 lipids, 260000 CG water molecules and 150*mM* salt (NaCl) with the box dimension of about 36.5nm × 36.5nm × 28nm. The membrane systems without MIM I-BAR have less water molecules (~106522) and smaller box (~36.5nm × 36.5nm × 13.8nm). For membrane systems with MIM I-BAR, we use a very large simulation box to make sure that MIM I-BAR can freely diffuse and rotate before binding onto the membrane (the longest dimension of MIM I-BAR dimer is around 19nm), which is important for non-biased membrane binding of MIM I-BAR. Lipids used herein include 1-palmitoyl-2-oleoyl-sn-glycero-3-phosphocholine (POPC), 1-palmitoyl-2-oleoyl-sn-glycero-3-phospho-L-serine (POPS), and PIP2. The MIM I-BAR dimer is initially placed parallel to and 8nm apart from the lipid membrane. To homogenize the distribution of molecules, all the systems built by *insane*[33] are firstly simulated at

temperature $T = 400K$ and the isobaric isothermal (NPT) ensemble for 100ns (The time reported in this work is the simulation time, and the corresponding effective time can be estimated after multiplying by 4.[31]) and then gradually reducing the temperature to 310K. Subsequent production simulations are performed for 10μs with the time step of 10fs and periodic boundary conditions.

For all simulations, a cutoff of 1.2 nm was used for van der Waals (vdW) interactions, and the Lennard-Jones potential was smoothly shifted to zero between 0.9 nm and 1.2 nm to reduce cutoff noise. For electrostatic interactions, the Columbic potential, with a cutoff of 1.2 nm, was smoothly shifted from 0 to 1.2 nm. The relative dielectric constant was 15, which is the default value of the force field [31]. Lipids, MIM I-BAR and water plus ions, were coupled separately to V-rescale heat baths[34] at $T = 310K$, with a coupling constant $\tau = 1\ ps$. The systems were simulated at 1 bar pressure using a semi-isotropic Parrinello-Rahman pressure coupling scheme[35] with a coupling constant $\tau = 5ps$ and compressibility of $3 \times 10^{-4}\ bar^{-1}$. The neighbor list for non-bonded interactions was updated every 10 steps with a cut-off of 1.2 nm. Snapshots of the simulation systems are rendered by VMD[36].

3. Results and discussion

Figure 1. **The amino acid sequence and structure of *Homo sapiens* MIM I-BAR used in the current work**. Amino acid sequence **(a)** and all-atom configuration shown in "Cartoon" **(b)** of MIM I-BAR with the coloring style: α-Helix (purple), 3_10_Helix (blue), Coil (white), Turn (cyan). The underlined amino acids are the differences between *Homo sapiens* and *Mus musculus* MIM I-BAR (Details can be found in **Fig. S1**). **(c)** Coarse-grained representation of MIM I-BAR dimer with backbone in pink and side-chain in yellow. The MIM I-BAR dimer is shown in the structure snapshots (b-c).

3.1 Coarse-grained Model of MIM I-BAR. In order to study the interactions between *Homo sapiens* MIM I-BAR and model membranes with Martini CG model[31, 37], the amino acid sequence (**Fig. 1a**) and the secondary structure of MIM I-BAR are necessary to construct the CG parameters for MIM I-BAR. However, the experimental crystal structure of *Homo sapiens* MIM is only available for its WH2 domain rather than the I-BAR domain.[19] Fortunately, the crystal structure of its homologous *Mus musculus* MIM I-BAR (PDB ID: 2D1L[19]) is available, which has a very similar amino acid sequence (**Fig. 1a and Fig. S1**) and therefore may have a similar structure to *Homo sapiens* MIM I-BAR. Hence, we obtain the atomistic structure of *Homo sapiens* MIM I-BAR (**Fig. 1b**) by performing homology modeling with MODELLER[38] using *Mus musculus* MIM I-BAR as a template. The secondary structure of *Homo sapiens* MIM I-BAR was then calculated using DSSP program on the atomic structure[39]. With the information of the amino acid sequence and the secondary structure, we generate the CG conformation (**Fig. 1c**) and parameters for *Homo sapiens* MIM I-BAR.

Figure 2. **The membrane binding affinity of MIM I-BAR is dependent on the concentration of PIP2 molecules**. **(a)** The side-view system snapshots of MIM I-BAR interacting with POPC membranes containing 0%, 5% and 15% PIP2 molecules at t=10μs. **(b)** The interaction energy and **(c)** number of contacts between MIM I-BAR and lipids. Mean ± s.e.m. is shown, based on the block average (eight blocks, block size: 500ns) over the last 4μs of 10μs MD trajectories. (d) The charge distribution on the surface of MIM I-BAR dimer.

3.2 PIP2 Plays Predominant Roles in the Membrane Binding of MIM I-BAR. To study the roles of PIP2 in the membrane binding of the MIM I-BAR, six membrane systems are used: one pure POPC bilayer, two asymmetric POPC/PIP2 membranes with 5% and 15% PIP2 in one membrane leaflet (**Fig. 2**), three asymmetric POPC/POPS membranes with 5%, 15% and 25% POPS in one leaflet (**Fig. 3**). MIM I-BAR dimer is placed adjacent to the membrane leaflet with PIP2 or POPS. **Fig. 2a** shows the last system snapshots of 10μs

CGMD simulation trajectories with different PIP2 concentrations. As shown, MIM I-BAR binds tightly onto the lipid membrane only in the presence of PIP2. Besides, the interaction energy (**Fig. 2b**) and contacts (**Fig. 2c**) between MIM I-BAR and the lipid membrane further reveal that the membrane binding ability of MIM I-BAR is dependent on the PIP2 concentration.

Figure 3. **The fingerprints of PIP2 on MIM I-BAR**. **(a)** Top-view snapshots of system POPC+15%PIP2: MIM I-BAR was shown in the left panel rather than the right, which indicates that the binding of MIM I-BAR onto the membrane can promote the PIP2 clustering around MIM I-BAR. **(b)** Probability distributions of PIP2 cluster sizes in the membrane system POPC+15%PIP2 with and without MIM I-BAR. **(c)** Coarse-grained configuration of MIM I-BAR with the color representing the contact probability with PIP2 molecules. **(d)** MIM I-BAR's residue-based contact probability with PIP2 molecules.

In order to quantify detailed interactions between MIM I-BAR and PIP2 molecules, we further focus on the system POPC+15%PIP2. As shown in the system snapshots (**Fig. 3a**), the membrane binding of MIM I-BAR can induce local PIP2 clustering. This somehow promotes the overall PIP2 clustering (**Fig. 3b**), which is consistent with the reported experiments of MIM I-BAR[40-41]. After further analyzing the direct contacts between MIM I-BAR and PIP2 molecules, we find that PIP2 binding sites are mainly located at two ends of the MIM I-BAR dimer (**Fig. 3c-d**), which reproduces the consistent contact fingerprints of PIP2 on the surface of MIM I-BAR as the PIP2-binding experiments by Mattila *et al.*[7] The consistency between our simulations and the reported experiments well validates the applicability of Martini CG model on the current work and our finding on the predominant roles of PIP2 in the membrane binding of MIM I-BAR.

Figure 4. **The membrane binding affinity of MIM I-BAR is not dependent on the concentration of POPS molecules**. **(a)** The system snapshots of MIM I-BAR interacting with POPC membranes with 0%, 5% and 15% POPS molecules at t=10μs. **(b)** The interaction energy and **(c)** number of contacts between MIM I-BAR and lipids. Mean ± s.e.m. is shown, based on the block average (eight blocks, size: 500ns) over the last 4μs of 10μs MD trajectories.

Considering the large negative charges on the PIP2's head-group and many positively charged residues on the surface of MIM I-BAR (**Fig. 2d**), electrostatic interactions may explain the predominant roles of PIP2 in the membrane binding of MIM I-BAR. Here, we also want to know membranes containing other negatively charged lipids (e.g. POPS, one major anionic lipid in plasma membrane) can have the similar ability to recruit MIM I-BAR. As shown in **Fig. 4a**, the binding affinity of MIM I-BAR with the membrane is not strong, and the membrane containing as high as 25% POPS still fails to fully recruit MIM I-BAR, which is consistent with the all-atom MD simulations of the interactions between the BAR-PH domain and the lipid membrane[42]. Quantifications of the detailed interactions (**Fig. 4b-c**) further indicate that MIM I-BAR has only one-fifth interaction strength with the lipid membrane of high POPS concentration (25%), compared to that with lipid membrane of the low PIP2 concentration (5%). Further increasing POPS concentration (15% → 25%) does not show any enhancement on the binding affinity of MIM I-BAR. In other words, POPS doesn't have comparable roles as PIP2 in the membrane binding of MIM I-BAR, which validates the predominant roles of PIP2 in this process.

Figure 5. The surface charge density maps of the membrane leaflets close to the MIM I-BAR for system POPC+25%POPS **(a)** and POPC+5%PIP2 **(b)** based on the first and the last 10ns of 10μs trajectories. The color represents different surface charge density as shown in the right color-bar. And such short time duration was chosen to reflect the transient charge density distribution in case the difference was averaged out over a long time period. Top-view snapshots of system POPC+25%POPS **(c)** and POPS+5%PIP2 **(d)**, where POPC is colored in green, POPS in blue and PIP2 in red.

For membrane systems POPC+25%POPS and POPC+5%PIP2, they have same total surface negative charges. However, as discussed above, the latter system shows the much better ability in recruiting MIM I-BAR. Here, we further explore the mechanism for the predominant roles of PIP2 in the membrane binding process of MIM I-BAR. As is known, POPS has only one net negative charge on its head-group, while PIP2 has five net negative charge on its head-group. Although the total surface charges are the same, the local distribution of these negative charges may greatly affect the local electrostatic interactions between MIM I-BAR and the lipid membrane, which determines the membrane binding process of MIM I-BAR. As shown in **Fig. 5**, compared to the POPS-containing membrane, the PIP2-contatining membrane can have much larger local surface charge density due to the transient and local PIP2 clustering. This local membrane patches of intensive negative charges can greatly strengthen the electrostatic interactions of MIM I-BAR with the lipid membrane and thus enhance the membrane binding process of MIM I-BAR. Besides, POPS has a much smaller head-group than PIP2 and is easier to be buried in the bulk membrane, which hinders the recognition by MIM I-BAR. All these points explain the molecular mechanism for the predominant roles of PIP2 in the membrane binding process of MIM I-BAR.

3.3 Membrane Curvature Promotes PIP2 Clustering in Negatively Curved Membrane Areas. As discussed above, we have uncovered the critical roles of PIP2 in the membrane binding of MIM I-BAR. However, whether PIP2 plays certain roles in the sensing negatively curved membranes of MIM I-BAR is still not clear. In order to elucidate this

question, we focus on the difference of PIP2 distribution between curved and planar membranes. First, an asymmetric lipid membrane without MIM I-BAR containing pure POPC in one membrane leaflet and 70% POPC, 25% POPS, 5% PIP2 in the other leaflet is built and run for 10μs. Then, a sufficient lateral pressure is added to the last frame of the planar membrane simulation trajectory to generate the curvature. The curved membrane system is also run for 10μs using the isothermal-isochoric (NVT) ensemble to keep the curvature. As shown in **Fig. 6a**, our curved membrane has both the negative and positive curvature at the PIP2 side, which enables the direct quantification of PIP2's preference to them. Both the side-view and top-view of our curved membrane indicate that PIP2 has the tendency to aggregate at the negatively curved membrane area (**Fig. 6a-b**). To validate this phenomenon, we count the number of different lipid molecules in both negatively and positively curved membrane areas (**Fig. 6c**), which correspond to the lower and upper halves of the curved membrane (The middle of the membrane is shown in light blue in **Fig. 6a**.). It is worth mention that the division from the center will make the positively curved membrane area larger than the negatively curved one. In other words, there will more lipids in total in the positively curved membrane (**Fig. 6c**). However, the negatively curved membrane area has more PIP2 molecules, which indicates larger PIP2 concentration in this area (5% in planar membrane) and smaller PIP2 concentration in positively curved membrane area. The enrichment of PIP2 in our negatively curved membrane shown here is consistent with the case of a much more complicated membrane reported by Kolds *et al*.[24] Although PIP2 has a large head-group, PIP2 used herein also contains a polyunsaturated acyl chain (arachidonic acid), which is very disordered, takes more space and thus redefines the lipid shape. This property tunes PIP2's preference to the negative curvature. Besides, using the script developed by Janosi *et al*.[43-45], we further quantify the detailed distribution of the PIP2 clusters. As shown in **Fig. 6d**, there is much more chance to have larger PIP2 clusters (no less

than 15 molecules). In other words, membrane curvature can re-distribute PIP2 molecules and promote the local enrichment and thus clustering of PIP2 molecules in negatively curved membrane areas. As discussed above, the membrane binding of MIM I-BAR positively correlates with the PIP2 concentration. This provides a reasonable explanation for how MIM I-BAR senses the negatively curved membrane.

Figure 6. Membrane Curvature induce the redistribution of PIP2. Side-view **(a)** and top-view **(b)** snapshots of the POPC (outer)-POPC/POPS/PIP2 (inner) curved membrane at t=10μs; POPC, POPS, PIP2 in the inner membrane leaflet are colored in green, blue and red correspondingly, while POPC in the outer leaflet is colored in pink. **(c)** Number of lipids in negatively and positively curved membrane areas (inner membrane leaflet) based on the block average (eight blocks, size: 500ns) over the last 4μs of 10μs trajectory, where mean ± s.e.m. is shown; **(d)** Probability distributions of PIP2 cluster sizes in the cases of curved and planar membranes.

As discussed above, our simulations have revealed the predominant roles of PIP2 in the membrane binding process of MIM I-BAR on molecular level (**Scheme 1**). PIP2 (one minor lipid in the plasma membrane) exerts much better ability in promoting the effective membrane binding of MIM I-BAR than POPS (one major anionic lipid). Meanwhile, the membrane binding of MIM I-BAR could in turn promote the local clustering of the surrounding PIP2 molecules at its two ends[46], which is crucial for the following membrane protrusion formation by synergistic interactions with actin proteins[7, 12, 19, 47]. On the other hand, the occurrence of membrane curvature can induce the re-distribution of lipids with the enrichment of PIP2 molecules at the negatively curved membrane areas (lower panel in **Scheme 1**). It is PIP2's preference to the negative membrane curvature that help elucidate how MIM I-BAR senses negatively curved membranes and helps maintain the membrane protrusion[7].

Scheme 1. **The unique roles of PIP2 in the membrane binding of MIM I-BAR**. PIP2 molecules are necessary to recruit MIM I-BAR, which in turn can induce local PIP2 clustering at its two end after binding onto the membrane (upper panel) and further contribute to the generation of membrane protrusions (right panel)[48]. Spontaneous bending of lipid membranes can re-distribute PIP2 molecules to the negatively curved membrane areas (lower panel), which promotes the recruitment of MIM I-BAR and maintaining the curvature (right panel)[48].

Conclusion

In this work, we have performed a series of 10μs-scale CGMD simulations to study the roles of PIP2 in the membrane binding of MIM I-BAR. Our results indicate that PIP2 plays an essential role in the membrane binding of MIM I-BAR in a concentration-dependent manner. In turn, MIM I-BAR can also induce the local PIP2 clustering at its two ends due to the preferred interactions between these residues and PIP2 molecules. The effective membrane binding of MIM I-BAR lays the foundation for the overall membrane protrusion process[7, 48]. On the other hand, we find that spontaneous membrane bending can induce the re-distribution of PIP2 molecules and promote the enrichment of PIP2 at negatively curved membrane areas. Considering these predominant roles of PIP2 in the membrane binding of MIM I-BAR, this finding can well explain how MIM I-BAR senses the negative curvature and helps maintain the membrane protrusions[48]. The insights provided by our simulations (**Scheme 1**) shed light on the molecular-level membrane binding process of MIM I-BAR, which is an effective supplement in understanding the roles of MIM I-BAR in generating and maintaining membrane protrusions.

Supporting Information

Additional figures and movies are available online.

Acknowledgements

We thank Prof. Steven (Xi) Zhan (University of Maryland) for helpful discussions. This work was supported by the National Natural Science Foundation of China (*Nos*. 61420106012, 61601227), National Basic Research Program of China (2013CB934400), the 111 Project (B13003), the Fundamental Research Funds for the Central Universities and the Collaborative Innovation Center of Suzhou Nano Science and Technology (SX21400213). We thank the Supercomputing Center of Beihang University and Southeast University and the Texas Advanced Computing Center (TACC) for generous computational resources.

References

1. Suetsugu, S.; Toyooka, K.; Senju, Y., Subcellular Membrane Curvature Mediated by the Bar Domain Superfamily Proteins. *Semin. Cell Dev. Biol.* **2010**, *21*, 340-349.
2. Suarez, A.; Ueno, T.; Huebner, R.; McCaffery, J. M.; Inoue, T., Bin/Amphiphysin/Rvs (Bar) Family Members Bend Membranes in Cells. *Sci. Rep.* **2014**, *4*.
3. Frost, A.; Unger, V. M.; De Camilli, P., The Bar Domain Superfamily: Membrane-Molding Macromolecules. *Cell* **2009**, *137*, 191-196.
4. Zhao, P.; Cao, M.; Song, L.; Wu, H.; Hu, K.; Chen, B.; Wang, Q.; Gu, N., Downregulation of Mim Protein Inhibits the Cellular Endocytosis Process of Magnetic Nanoparticles in Macrophages. *RSC Advances* **2016**, *6*, 96635-96643.
5. Peter, B. J.; Kent, H. M.; Mills, I. G.; Vallis, Y.; Butler, P. J. G.; Evans, P. R.; McMahon, H. T., Bar Domains as Sensors of Membrane Curvature: The Amphiphysin Bar Structure. *Science* **2004**, *303*, 495-499.
6. Itoh, T.; Erdmann, K. S.; Roux, A.; Habermann, B.; Werner, H.; De Camilli, P., Dynamin and the Actin Cytoskeleton Cooperatively Regulate Plasma Membrane Invagination by Bar and F-Bar Proteins. *Dev. Cell* **2005**, *9*, 791-804.
7. Mattila, P. K.; Pykäläinen, A.; Saarikangas, J.; Paavilainen, V. O.; Vihinen, H.; Jokitalo, E.; Lappalainen, P., Missing-in-Metastasis and Irsp53 Deform Pi (4, 5) P2-Rich Membranes by an Inverse Bar Domain–Like Mechanism. *J. Cell Biol.* **2007**, *176*, 953-964.
8. Blood, P. D.; Voth, G. A., Direct Observation of Bin/Amphiphysin/Rvs (Bar) Domain-Induced Membrane Curvature by Means of Molecular Dynamics Simulations. *Proc. Natl. Acad. Sci. U. S. A.* **2006**, *103*, 15068-15072.
9. Blood, P. D.; Swenson, R. D.; Voth, G. A., Factors Influencing Local Membrane Curvature Induction by N-Bar Domains as Revealed by Molecular Dynamics Simulations. *Biophys. J.* **2008**, *95*, 1866-1876.

10. Yin, Y.; Arkhipov, A.; Schulten, K., Simulations of Membrane Tubulation by Lattices of Amphiphysin N-Bar Domains. *Structure* **2009**, *17*, 882-892.

11. Arkhipov, A.; Yin, Y.; Schulten, K., Four-Scale Description of Membrane Sculpting by Bar Domains. *Biophys. J.* **2008**, *95*, 2806-2821.

12. Saarikangas, J.; Mattila, P. K.; Varjosalo, M.; Bovellan, M.; Hakanen, J.; Calzada-Wack, J.; Tost, M.; Jennen, L.; Rathkolb, B.; Hans, W., Missing-in-Metastasis Mim/Mtss1 Promotes Actin Assembly at Intercellular Junctions and Is Required for Integrity of Kidney Epithelia. *J. Cell. Sci.* **2011**, *124*, 1245-1255.

13. Chen, Z.; Shi, Z.; Baumgart, T., Regulation of Membrane-Shape Transitions Induced by I-Bar Domains. *Biophys. J.* **2015**, *109*, 298-307.

14. Cao, M.; Ye, Z.; Lin, X.; Gu, N., Advances in Missing-in-Metastasis Research. *Chin. Sci. Bull.* **2015**, *60*, 356-366.

15. Lee, Y.-G.; Macoska, J. A.; Korenchuk, S.; Pienta, K. J., Mim, a Potential Metastasis Suppressor Gene in Bladder Cancer. *Neoplasia* **2002**, *4*, 291-294.

16. Yu, D.; Zhan, X. H.; Zhao, X. F.; Williams, M. S.; Carey, G. B.; Smith, E.; Scott, D.; Zhu, J.; Guo, Y.; Cherukuri, S., Mice Deficient in Mim Expression Are Predisposed to Lymphomagenesis. *Oncogene* **2012**, *31*, 3561-3568.

17. Parr, C.; Jiang, W. G., Metastasis Suppressor 1 (Mtss1) Demonstrates Prognostic Value and Anti-Metastatic Properties in Breast Cancer. *Eur. J. Cancer* **2009**, *45*, 1673-1683.

18. Liu, K.; Wang, G.; Ding, H.; Chen, Y.; Yu, G.; Wang, J., Downregulation of Metastasis Suppressor 1 (Mtss1) Is Associated with Nodal Metastasis and Poor Outcome in Chinese Patients with Gastric Cancer. *BMC Cancer* **2010**, *10*, 1.

19. Lee, S. H.; Kerff, F.; Chereau, D.; Ferron, F.; Klug, A.; Dominguez, R., Structural Basis for the Actin-Binding Function of Missing-in-Metastasis. *Structure* **2007**, *15*, 145-155.

20. Cao, M.; Zhan, T.; Ji, M.; Zhan, X., Dimerization Is Necessary for Mim-Mediated Membrane Deformation and Endocytosis. *Biochem. J.* **2012**, *446*, 469-475.

21. Cao, M.; Chang, W.; Zheng, M.; Xie, L.; Zhang, Y.; Cai, J.; Chen, J.; Zhan, X.; Ji, M.; Gu, N., Design of Small Molecules Targeting I-Bar Proteins. *Curr. Pharm. Des.* **2015**, *21*, 1318-1326.

22. Zhang, Y.; Lou, Z.; Lin, X.; Wang, Q.; Cao, M.; Gu, N., Optimizing Purification Process of Mim-I-Bar Domain by Introducing Atomic Force Microscope and Dynamics Simulations. *Colloids Surf. B Biointerfaces* **2017**, *157*, 391-397.

23. Di Paolo, G.; De Camilli, P., Phosphoinositides in Cell Regulation and Membrane Dynamics. *Nature* **2006**, *443*, 651-657.

24. Koldsø, H.; Shorthouse, D.; Hélie, J.; Sansom, M. S., Lipid Clustering Correlates with Membrane Curvature as Revealed by Molecular Simulations of Complex Lipid Bilayers. *PLoS Comput. Biol.* **2014**, *10*, e1003911.

25. Lin, X.; Gu, N., Surface Properties of Encapsulating Hydrophobic Nanoparticles Regulate the Main Phase Transition Temperature of Lipid Bilayers: A Simulation Study. *Nano Res.* **2014**, *7*, 1195-1204.

26. Lin, X.; Zhang, S.; Ding, H.; Leventa, I.; Gorfe, A. A., The Aliphatic Chain of Cholesterol Modulates Bilayer Interleaflet Coupling and Domain Registration. *FEBS Lett.* **2016**, *590*, 3368-3374.

27. Periole, X.; Knepp, A. M.; Sakmar, T. P.; Marrink, S. J.; Huber, T., Structural Determinants of the Supramolecular Organization of G Protein-Coupled Receptors in Bilayers. *J. Am. Chem. Soc.* **2012**, *134*, 10959-10965.

28. Schäfer, L. V.; de Jong, D. H.; Holt, A.; Rzepiela, A. J.; de Vries, A. H.; Poolman, B.; Killian, J. A.; Marrink, S. J., Lipid Packing Drives the Segregation of Transmembrane Helices into Disordered Lipid Domains in Model Membranes. *Proc. Natl. Acad. Sci. U. S. A.* **2011**, *108*, 1343-1348.

29. Chavent, M.; Duncan, A. L.; Sansom, M. S., Molecular Dynamics Simulations of Membrane Proteins and Their Interactions: From Nanoscale to Mesoscale. *Curr. Opin. Struct. Biol.* **2016**, *40*, 8-16.

30. Lin, X.; Zuo, Y. Y.; Gu, N., Shape Affects the Interactions of Nanoparticles with Pulmonary Surfactant. *Sci. China Mater.* **2015**, *58*, 28-37.

31. Marrink, S. J.; Risselada, H. J.; Yefimov, S.; Tieleman, D. P.; De Vries, A. H., The Martini Force Field: Coarse Grained Model for Biomolecular Simulations. *J. Phys. Chem. B* **2007**, *111*, 7812-7824.

32. Abraham, M. J.; Murtola, T.; Schulz, R.; Páll, S.; Smith, J. C.; Hess, B.; Lindahl, E., Gromacs: High Performance Molecular Simulations through Multi-Level Parallelism from Laptops to Supercomputers. *SoftwareX* **2015**, *1*, 19-25.

33. Wassenaar, T. A.; Ingólfsson, H. I.; Böckmann, R. A.; Tieleman, D. P.; Marrink, S. J., Computational Lipidomics with Insane: A Versatile Tool for Generating Custom Membranes for Molecular Simulations. *J. Chem. Theory Comput.* **2015**, *11*, 2144-2155.

34. Bussi, G.; Donadio, D.; Parrinello, M., Canonical Sampling through Velocity Rescaling. *J. Chem. Phys.* **2007**, *126*, 014101.

35. Parrinello, M.; Rahman, A., Polymorphic Transitions in Single Crystals: A New Molecular Dynamics Method. *J. Appl. Phys.* **1981**, *52*, 7182-7190.

36. Humphrey, W.; Dalke, A.; Schulten, K., Vmd: Visual Molecular Dynamics. *J. Mol. Graph.* **1996**, *14*, 33-38.

37. Monticelli, L.; Kandasamy, S. K.; Periole, X.; Larson, R. G.; Tieleman, D. P.; Marrink, S. J., The Martini Coarse-Grained Force Field: Extension to Proteins. *J. Chem. Theory Comput.* **2008**, *4*, 819-834.

38. Fiser, A.; Šali, A., Modeller: Generation and Refinement of Homology-Based Protein Structure Models. *Methods Enzymol.* **2003**, *374*, 461-491.

39. Kabsch, W.; Sander, C., Dictionary of Protein Secondary Structure: Pattern Recognition of Hydrogen - Bonded and Geometrical Features. *Biopolymers* **1983**, *22*, 2577-2637.

40. Saarikangas, J.; Zhao, H.; Pykäläinen, A.; Laurinmäki, P.; Mattila, P. K.; Kinnunen, P. K.; Butcher, S. J.; Lappalainen, P., Molecular Mechanisms of Membrane Deformation by I-Bar Domain Proteins. *Curr. Biol.* **2009**, *19*, 95-107.

41. Zhao, H.; Pykäläinen, A.; Lappalainen, P., I-Bar Domain Proteins: Linking Actin and Plasma Membrane Dynamics. *Curr. Opin. Cell Biol.* **2011**, *23*, 14-21.

42. Chan, K. C.; Lu, L.; Sun, F.; Fan, J., Molecular Details of the Ph Domain of Acap1bar-Ph Protein Binding to Pip-Containing Membrane. *J. Phys. Chem. B* **2017**, *121*, 3586-3596.

43. Janosi, L.; Li, Z.; Hancock, J. F.; Gorfe, A. A., Organization, Dynamics, and Segregation of Ras Nanoclusters in Membrane Domains. *Proc. Natl. Acad. Sci. U. S. A.* **2012**, *109*, 8097-8102.

44. Li, Z.; Janosi, L.; Gorfe, A. A., Formation and Domain Partitioning of H-Ras Peptide Nanoclusters: Effects of Peptide Concentration and Lipid Composition. *J. Am. Chem. Soc.* **2012**, *134*, 17278-17285.

45. Lin, X.; Li, Z.; Gorfe, A. A., Reversible Effects of Peptide Concentration and Lipid Composition on H-Ras Lipid Anchor Clustering. *Biophys. J.* **2015**, *109*, 2467-2470.

46. McLaughlin, S.; Wang, J.; Gambhir, A.; Murray, D., Pip2 and Proteins: Interactions, Organization, and Information Flow. *Annu. Rev. Biophys. Biomol. Struct.* **2002**, *31*, 151-175.

47. Yu, D.; Zhan, X. H.; Niu, S.; Mikhailenko, I.; Strickland, D. K.; Zhu, J.; Cao, M.; Zhan, X., Murine Missing in Metastasis (Mim) Mediates Cell Polarity and Regulates the Motility Response to Growth Factors. *PloS one* **2011**, *6*, e20845.

48. Prévost, C.; Zhao, H.; Manzi, J.; Lemichez, E.; Lappalainen, P.; Callan-Jones, A.; Bassereau, P., Irsp53 Senses Negative Membrane Curvature and Phase Separates Along Membrane Tubules. *Nat. Commun.* **2015**, *6*, 8529.